JOURNAL OF GUIDANCE, CONTROL, AND DYNAMICS
Vol. 31, No. 6, November–December 2008

Effects of Peripheral Visual and Physical Motion Cues in Roll-Axis Tracking Tasks

D. M. Pool,* M. Mulder,† M. M. Van Paassen,‡ and J. C. Van der Vaart§
Delft University of Technology, 2600 GB Delft, The Netherlands

DOI: 10.2514/1.36334

In this paper, the effects of peripheral visual and physical motion cues on manual control of second-order roll dynamics are investigated. In particular, the differences between the use of these cues in compensatory target-following and disturbance-rejection tasks are considered. Tracking performance, control activity, and measures of control behavior are determined from recent measurements and compared with results from an earlier experiment. Most previously reported effects of peripheral visual and physical motion cues in target following and disturbance rejection are confirmed. A comparison of tasks with varying levels of difficulty is found to reveal reduced effectiveness of peripheral visual and physical motion cues in the less difficult target-following tasks only. Observed differences in measured control behavior for target following and disturbance rejection are related to effective strategies for reducing tracking errors introduced by the forcing-function signals in both tasks.

Nomenclature

A_f	=	signal amplitude distribution
e	=	tracking error
f	=	forcing function
f_d	=	disturbance forcing function
f_t	=	target forcing function
$H_c(j\omega)$	=	controlled system frequency response
$H_{\text{ol}}(j\omega)$	=	open-loop frequency response
$H_p(j\omega)$	=	equivalent pilot frequency response
$H_{p_e}(j\omega)$	=	pilot frequency response with respect to e
$H_{p_\phi}(j\omega)$	=	pilot frequency response with respect to ϕ
K_{p_ϕ}	=	pilot ϕ response gain
n	=	pilot remnant
$r_{e,u}$	=	relative control effort
$S_{nn}(j\omega)$	=	remnant spectrum
$S_{uu}(j\omega)$	=	control signal spectrum
t	=	time
u	=	control manipulator deflection
ρ^2	=	correlation coefficient
τ_e	=	equivalent time delay
ϕ	=	roll angle
ϕ_f	=	signal phase distribution
φ_m	=	phase margin
ω	=	frequency
ω_c	=	unit gain crossover frequency

Subscripts

d	=	disturbance rejection
i	=	forcing-function sinusoid index
t	=	target following
1	=	experiment forcing function 1
2	=	experiment forcing function 2

I. Introduction

THE interaction of visual and physical motion perception in closed-loop manual vehicle control is a subject that has received considerable attention. Numerous studies are described that investigate the influence of human visual and physical motion perception on performance and manual control behavior in a myriad of control tasks [1–11].

Many considered manual control behavior for one of two different types of compensatory tracking task: target following and disturbance rejection. In a target-following task, the objective is to make the controlled variable follow a target signal; for disturbance rejection, the effect of a disturbance signal is counteracted. The target and disturbance signals considered in such experiments are generally quasi-random. Results of early investigations into the effects of peripheral visual and physical motion cues on vehicle control indicate that these cues are used differently for target-following and disturbance-rejection tasks [2,5,6].

The amount of experimental data that support these observations, however, are limited, and experimental results are often hard to compare because of large differences in apparatus, vehicle dynamics, task definition, and task difficulty. To draw more definitive conclusions on the effects of peripheral visual and physical motion cues in target following and disturbance rejection and to gather a significant body of data, Hosman and Van der Vaart [7–9] performed an extensive experiment in which both tasks were considered for control of aircraft roll attitude. This experiment has acted as a benchmark for later research on simulator fidelity and motion cueing [12–15] and modeling human motion perception [11,16–19].

The purpose of this study was to investigate the effects of visual and physical motion cues on manual roll-axis control for compensatory tracking tasks by verification of (and possible addition to) the results documented by Hosman and Van der Vaart [7–9]. The focus of the current research is twofold. First, the inherent differences between the use of these cues for compensatory target following and disturbance rejection will be identified. Second, the effect of task difficulty on the observed trends in performance and control behavior is evaluated by considering target and disturbance signals with different spectra for both tasks.

Presented as Paper 6896 at the AIAA Modeling and Simulation Technologies Conference and Exhibit, Hilton Head, SC, 20–23 August 2007; received 24 December 2007; revision received 25 February 2008; accepted for publication 3 March 2008.

*Ph.D. Candidate, Control and Simulation Division, Faculty of Aerospace Engineering, P.O. Box 5058; d.m.pool@tudelft.nl. Student Member AIAA.

†Associate Professor, Control and Simulation Division, Faculty of Aerospace Engineering, P.O. Box 5058; m.mulder@tudelft.nl. Member AIAA.

‡Associate Professor, Control and Simulation Division, Faculty of Aerospace Engineering, P.O. Box 5058; m.m.vanpaassen@tudelft.nl. Member AIAA.

§Associate Professor, Control and Simulation Division, Faculty of Aerospace Engineering, P.O. Box 5058; j.c.vandervaart@tudelft.nl.

II. Compensatory Target Following and Disturbance Rejection

Compensatory tracking tasks require the active minimization of a deviation from a desired state or trajectory. Generally, only the tracking error is presented on a visual display [20,21]. Certain aspects of manual aircraft control involve compensatory tracking. For instance, performing an instrument landing system approach requires a pilot to continuously minimize the deviations from the desired approach path shown on his glide slope indicator. Maintaining a certain aircraft attitude in atmospheric turbulence is another example. It is likely that peripheral visual and physical motion sensations aid in the minimization of the compensatory error in such situations. The precise function and effect of these extra cues may vary from task to task, however.

A. Inherent Differences Between Target Following and Disturbance Rejection

In compensatory tracking, a distinction can be made between target-following and disturbance-rejection tasks [8,9]. In target following, the goal is to ensure that the controlled variable follows a time-varying reference signal. In disturbance rejection, this reference state is constant (usually zero), but the pilot has to compensate for the deviations introduced by the disturbance signal.

Pilot control behavior in manual tracking tasks is generally modeled as a linear response to perceived variables and a remnant signal n that accounts for nonlinear and noise contributions [20,21]. In Fig. 1, H_{p_e} indicates the linear response to the compensatory error signal e and H_c represents the controlled system dynamics; f_t and f_d denote the target and disturbance signals or forcing functions, respectively.

The two task structures shown in Fig. 1 represent target-following and disturbance-rejection tasks that are performed with a compensatory visual display only; just the error signal e is presented. In this case, with a proper choice of the target and disturbance signals' spectra, the tasks are in fact equivalent and indistinguishable by the pilot, because the control action u is a reaction to a displayed error only. When compensatory tracking of the roll angle ϕ in actual flight is considered, however, peripheral visual and physical motion cues provide additional feedback of roll attitude and its derivatives. This is depicted in Fig. 2, in which a second linear pilot response, H_{p_ϕ}, is added to the pilot control model.

Figure 2b shows that in disturbance rejection, the signals perceived from the compensatory display and from extra physical or peripheral visual motion cues are the same due to the absence of a target signal: both are equal to the (negative) roll angle ϕ. This implies that in compensatory disturbance rejection, the different pilot perception processes work *in parallel* and can be expected to yield enhanced perception of the controlled roll attitude.

In compensatory target following (Fig. 2a), the information perceived from the peripheral visual field and physical motion sensations does *not* correspond to the information shown on the central display, due to the presence of a nonzero target signal f_t. Here, additional motion cues do not yield parallel perception of the controlled variable (the error signal e), but instead give pilots feedback on the aircraft roll motion caused by their control action u.

Summarizing, it is likely that peripheral visual and physical motion cues serve a different purpose in compensatory target-following and disturbance-rejection tasks. This also has consequences for interpreting changes in measured control behavior for these tasks.

B. Stability Characteristics for Target Following and Disturbance Rejection

Crossover frequency and phase margin are often used as the main characteristic variables of human control behavior in manual tracking tasks [20,21]. These classical control-theoretic properties of the open-loop response are representative of the characteristics of the corresponding closed-loop system. For compensatory tracking tasks with only a compensatory display, the open-loop transfer function $H_{\text{ol}}(j\omega)$ is easily deduced from Fig. 1 and equal to $H_{p_e}(j\omega)H_c(j\omega)$ for both target following and disturbance rejection.

For compensatory tracking tasks in which peripheral visual and physical motion cues are available, the different function of these extra cues in target following and disturbance rejection yields different expressions for the open-loop transfer function. Expressions for the equivalent pilot describing function $H_p(j\omega)$ can be derived for both tasks by restructuring the block diagrams in Fig. 2 to single-loop unity feedback control systems.

Target following:

$$H_p(j\omega) = \frac{U(j\omega)}{E(j\omega)} = \frac{H_{p_e}(j\omega)}{1 + H_{p_\phi}(j\omega)H_c(j\omega)} \tag{1}$$

Disturbance rejection:

$$H_p(j\omega) = \frac{U(j\omega)}{E(j\omega)} = H_{p_e}(j\omega) + H_{p_\phi}(j\omega) \tag{2}$$

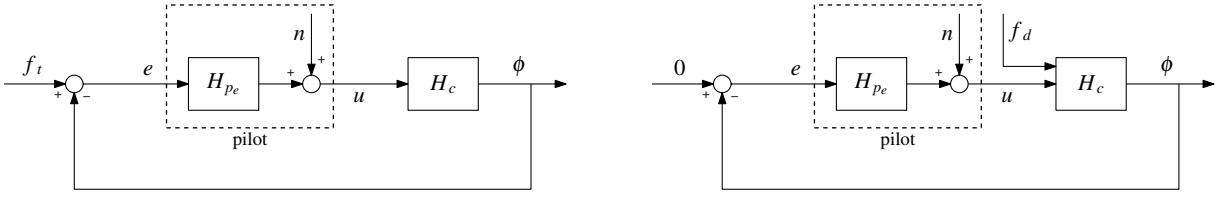

a) Target-following task b) Disturbance-rejection task

Fig. 1 Compensatory target-following and disturbance-rejection tasks, with central visual display only.

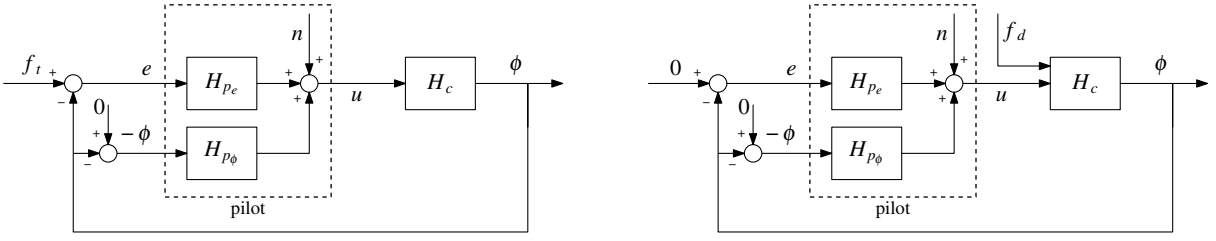

a) Target-following task b) Disturbance-rejection task

Fig. 2 Compensatory target-following and disturbance-rejection tasks, with additional peripheral and physical motion cues.

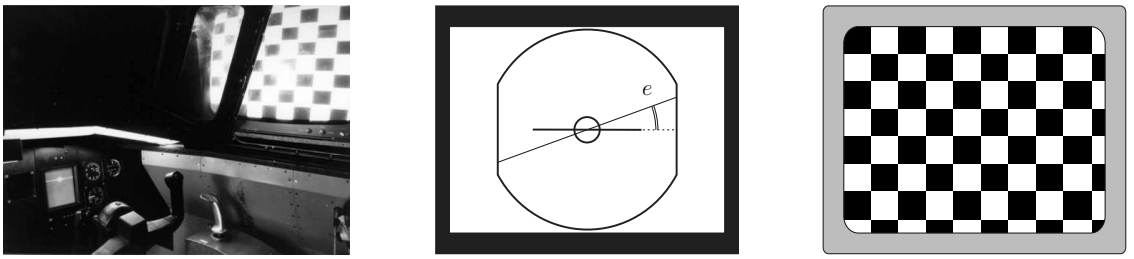

a) Simulator cockpit b) Central display c) Peripheral display

Fig. 3 Simulator cockpit and displays used in the Van der Vaart [8] tracking experiment.

The corresponding open-loop dynamics for both tasks are defined by the product of $H_p(j\omega)$ and the controlled system dynamics: $H_{\text{ol}}(j\omega) = H_p(j\omega)H_c(j\omega)$. Substitution of Eq. (1) for target following, or Eq. (2) for disturbance rejection, yields different open-loop expressions. Even if pilot characteristics $H_{p_e}(j\omega)$ and $H_{p_\phi}(j\omega)$ are *equal* for both tasks, they result in a *different* open-loop response in target following and disturbance rejection. This also affects related open-loop metrics such as crossover frequency and phase margin, which will be evaluated in more detail in Sec. V.B.2.[¶]

III. Hosman and Van der Vaart Tracking Experiment

To evaluate the effects of peripheral visual and physical motion cues in compensatory roll-axis tracking, a simulator tracking experiment was performed. This experiment can, to a large extent, be seen as a replication of an earlier experiment performed at the Delft University of Technology (TU Delft) by Hosman [9] and Van der Vaart [8]. Before elaborating on the new experiment, a short overview of the original experiment is provided in this section.

A. Tracking Task and Variation of Motion Cues

Hosman and Van der Vaart [7–9] studied compensatory tracking for aircraft roll attitude. The controlled system dynamics were defined by a double integrator [i.e., $H_c(j\omega) = K_c/(j\omega)^2$, with $K_c = 4$], yielding a roll acceleration of 4 deg/s^2 for every degree of control deflection u. For generating control inputs, a side stick manipulator was used.

For control of the aircraft roll angle ϕ, it was hypothesized that in actual flight, pilots use motion information from three different sources:

1) The perception of roll *attitude* and *rate* is from a central visual instrument display C.

2) The perception of roll *rate* is from the peripheral visual field P.

3) The perception of roll *acceleration* and lateral specific force are from physical motion M.

The individual and combined effects of motion cues from these three different sources (C, P, and M) were investigated by systematically varying their availability in a simulator environment. These experimental conditions will hereby be referred to using an acronym that indicates which motion cues were available. For instance, the condition in which physical motion cues were provided in addition to the central visual cues is indicated with the abbreviation CM. The baseline condition was the situation in which only the central instrument display (depicting a simplified artificial horizon image, as shown in Fig. 3b) was available.

Subjects were seated in the right pilot station. Additional peripheral visual cues were generated using two 60-Hz TV monitors that were mounted outside of the simulator's side windows (Fig. 3a). Vertically moving checkerboard patterns (9.5 by 7.5 blocks) provided a sensation of roll motion without giving a roll-attitude reference (see Fig. 3c). A three-degree-of-freedom (heave, pitch, and roll) moving-base simulator was used for generating physical motion cues. Pure roll motion cues were provided during the experiment (no washout).

Three jet aircraft pilots performed the experiment. They were extensively trained (over 400 runs combined) to ensure stable performance before the measurements were taken. Each measurement run lasted 104 s, of which the final 81.92 s were analyzed. These were used to evaluate the effect of peripheral visual and physical motion cues on tracking performance, control activity, and pilot control behavior.

B. Forcing Function

Together with the controlled system dynamics, the applied target or disturbance forcing-function signals (FS) largely determine tracking-task difficulty [20,21]. A pseudorandom forcing-function signal was constructed as a sum of ten sinusoids:

$$f(t) = \sum_{i=1}^{10} A_f(\omega_i)\sin(\omega_i t + \phi_f(\omega_i)) \tag{3}$$

where $A_f(\omega_i)$ and $\phi_f(\omega_i)$ are the amplitude and phase shift distributions, respectively. The frequencies ω_i were similar to the values used by McRuer et al. [20] in their tracking experiments (i.e., more or less evenly distributed over the frequency range of 0.153 to 13.576 rad/s). For the amplitude distribution $A_f(\omega_i)$, a first-order low-pass filter with time constant $\tau_f = 0.6$ s and gain $K_f = 1.11$ was used: $A_f(\omega_i) = |K_f/(1 + \tau_f j\omega_i)|$.

One set of randomly selected phases $\phi_f(\omega_i)$ was defined, yielding a single forcing-function signal realization. Note that Hosman and Van der Vaart [7–9] used this forcing function, indicated with the symbol f_1 in the remainder of this paper, as *both* their target-following and disturbance-rejection-task forcing function (f_t and f_d in Figs. 1 and 2). As later remarked by Van der Vaart [8], this choice had major consequences for the experimental results.

C. Main Experimental Results

Hosman and Van der Vaart [7–9] found that the addition of peripheral visual and physical motion cues led to better tracking performance and lower control activity, in both target-following and disturbance-rejection tasks. The effect of physical motion cues was significantly larger than that of peripheral visual cues, especially in disturbance tasks, in which the effect of peripheral visual cues was found to be relatively minor.

To investigate changes in control behavior that resulted from the addition of extra motion cues, Hosman and Van der Vaart [7–9] evaluated measured equivalent pilot describing functions $H_p(j\omega)$. The averaged frequency response functions, calculated from measured control and tracking-error-signal time histories according to Eqs. (1) and (2), are depicted in Fig. 4.

For target following, the addition of peripheral visual and physical motion cues reduced the pilot gain (Fig. 4a) and greatly increased the low-frequency phase lead generated by the pilot (Fig. 4c). In disturbance rejection, a significant increase in pilot gain was found for the addition of physical motion cues, accompanied by an increase

[¶]Note that for tasks without peripheral visual or physical motion feedback $H_{p_\phi}(j\omega) = 0$ and both Eqs. (1) and (2) simplify to $H_p(j\omega) = H_{p_e}(j\omega)$. So direct comparison of target-following and disturbance-rejection stability characteristics is valid for tasks with just a compensatory visual display.

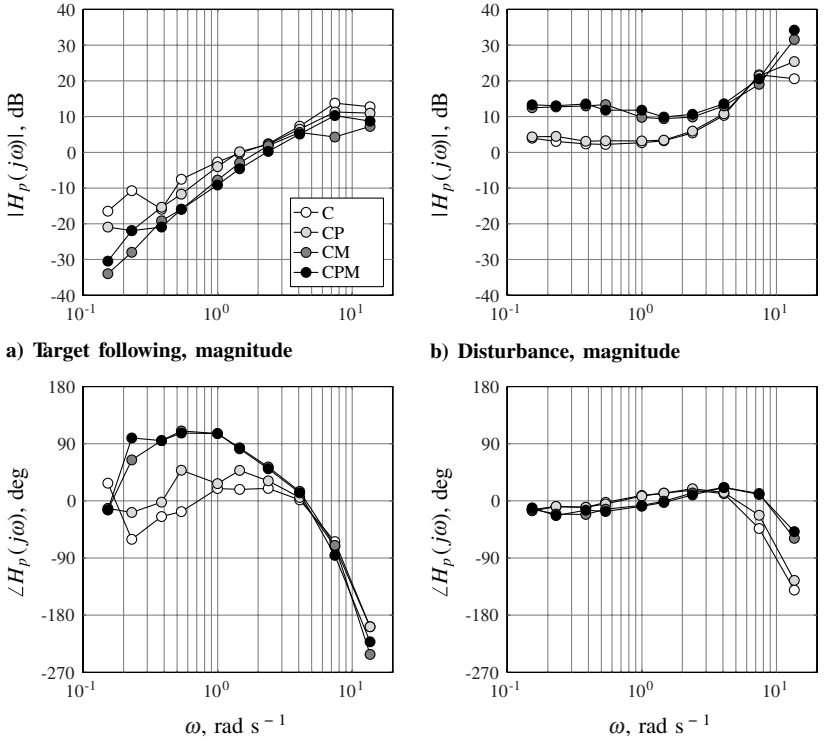

a) Target following, magnitude b) Disturbance, magnitude

c) Target following, phase d) Disturbance, phase

Fig. 4 Averaged pilot describing functions measured by Van der Vaart [8].

in high-frequency phase lead, as shown in Figs. 4b and 4d, respectively.

The main results of the Hosman and Van der Vaart [7–9] experiment (i.e., similar trends in tracking performance and control activity and opposite trends in control behavior) were regarded as representative effects of adding peripheral visual and physical motion cues in compensatory target-following and disturbance-rejection tasks. As indicated earlier, these tracking tasks are in fact indistinguishable when performed with only a compensatory display (condition C). As can be judged from Fig. 4, significant differences in control behavior were found, however, for this condition. This artifact can be explained by reviewing the block diagrams of both tasks in Fig. 1.

Recall that Hosman and Van der Vaart [7–9] defined one forcing function: f_1. This signal was used as f_t in their target-following tasks and as f_d in their disturbance-rejection tasks. Whereas in target following, f_t drives the error signal e directly, in disturbance rejection, the forcing function f_d first travels through the system dynamics $H_c(j\omega)$ before being presented to the pilot. Because $H_c(j\omega)$ was a double integrator, the disturbance signal was integrated twice before its effect could be perceived from the compensatory display, greatly attenuating its high-frequency content. This lower bandwidth of the effectively controlled disturbance signal caused the disturbance task to be much easier to perform than the target-following task.

D. Discrepancy in Target-Following and Disturbance-Task Difficulty

Tracking-task difficulty can have a major effect on the adopted control behavior. McRuer et al. [20,21] investigated the effect of forcing-function bandwidth and controlled dynamics (two factors that largely determine task difficulty) on manual control behavior. For control of double-integrator dynamics, McRuer et al. reported similar control behavior for all three of their forcing-function spectra, except the one with the highest bandwidth. Here, subjects showed a reduction in the bandwidth of their control action, because they were no longer able to achieve stable control over the higher frequencies in the signal. McRuer et al. called this phenomenon, which is characterized by a reduction in crossover frequency, *crossover regression*.

The first-order amplitude distribution used by Hosman and Van der Vaart [7–9] yields a signal with relatively high power at the higher sinusoid frequencies. In fact, from comparison with the forcing-function signals used by McRuer et al. [20], it would be likely that the forcing function f_1 would cause crossover regression in the control of a second-order system. In disturbance rejection, however, the attenuation of the high-frequency power by $H_c(j\omega)$ would yield an effectively reduced forcing-function bandwidth, in which crossover regression would not be necessary.

In Fig. 5, the crossover frequencies measured by Hosman and Van der Vaart [7–9] for both tasks are depicted. Changes in crossover frequency correspond well to the observed changes in the magnitude of $H_p(j\omega)$ for both types of task. For the condition with a central display only (C), the target-following crossover frequency is much lower than for the corresponding disturbance-rejection task. Apparently, the discrepancy in task difficulty between both tasks led pilots to regress their crossover frequency in the target-following task *only*.

In conclusion, the differences observed by Hosman and Van der Vaart [7–9] in target-following and disturbance-rejection control behavior, as shown in Figs. 4 and 5, may in fact be partly attributed to the difference in task difficulty, instead of resulting from the inherent differences between both tasks. This motivated a replication of the experiment.

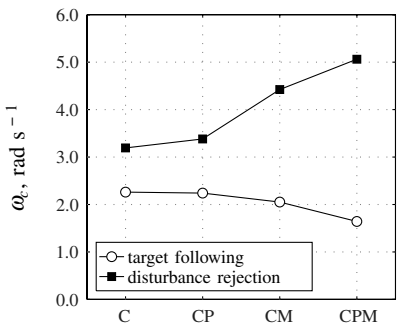

Fig. 5 Crossover frequencies measured by Van der Vaart [8].

IV. Experiment Setup

To investigate to what extent the discrepancy in baseline task difficulty has affected the conclusions on pilot tracking performance and control behavior drawn from the Hosman and Van der Vaart [7–9] tracking experiment, a similar experiment was performed in the new simulator at TU Delft. Considerable effort was put into making most experimental variables as equal as possible to those of the original experiment, to ensure that a meaningful comparison of experimental results could be made. The most important deviations from the tracking experiment performed by Hosman and Van der Vaart [7–9] and the reasons for them will be described next.

A. Simulator and Generation of Visual and Physical Motion Cues

The experiment was performed in a different moving-base simulator: TU Delft's six-degree-of-freedom simulation, motion, and navigation (SIMONA) research simulator (Fig. 6a). Instead of using TV monitors to generate the peripheral visual cues in the SIMONA research simulator, the moving checkerboard patterns were projected on SIMONA's outside visual display. Figure 6b shows the right pilot station, illustrating the right-hand-side checkerboard pattern. For these projected checkerboard patterns, it was ensured that their positions in the subjects' fields of view approximated those of the TV monitors in the Hosman and Van der Vaart [7–9] experiment. The update rate of the checkerboard pattern was 60 Hz; the time delay was measured to be on the order of 25–30 ms [22].

Figure 6b shows the compensatory artificial horizon display, presented on an liquid crystal display monitor with an update rate of 60 Hz and a time delay of 20–25 ms. Figure 6b also shows the electronic side stick that is mounted at the right pilot station. The stick was calibrated to have force-displacement characteristics equal to those in the original experiment [9].

For presenting the roll-axis physical motion cues, SIMONA's motion system was used. To generate pilot head accelerations that were equivalent to those provided in the original experiment, extra heave and sway motion was implemented, because the distance between SIMONA's roll axis and the right pilot station was slightly larger. The delay in generating the physical motion cues was approximately 30 ms [23].

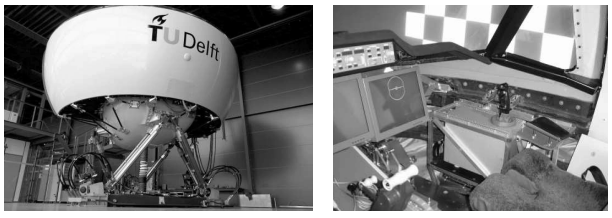

a) b)

Fig. 6 The SIMONA research simulator and a view of its right pilot station.

B. Target-Following and Disturbance-Rejection Tasks of Equal Difficulty

To achieve a target-following and disturbance-rejection task of equal difficulty, one should aim for the same spectrum or bandwidth of the error signal e, the signal presented on the compensatory display. Although each task can be adapted to the level of difficulty of the other [8], demands on a target forcing function are more stringent, because in conditions with physical motion cues, the simulator will follow a trajectory approximately equal to f_t. For this reason, the disturbance-rejection tasks in this experiment were adapted to the level of difficulty of the corresponding target-following tasks, as illustrated in Fig. 7.

The adapted disturbance task shown in Fig. 7b was implemented by generating a disturbance forcing function f_d, of which the amplitudes were scaled with the inverse of the magnitude of H_c at the corresponding sinusoid frequencies:**

$$f_d(t) = \sum_{i=1}^{10} \frac{\omega_i^2 A_f(\omega_i)}{K_c} \sin(\omega_i t + \phi_f(\omega_i)) \tag{4}$$

The target forcing function f_t was defined using Eq. (3).

C. Forcing Functions

To ensure that a meaningful comparison with the results of the original experiment could be made, exactly the same forcing function as devised by Hosman and Van der Vaart [7–9], f_1, was used [$\tau_f = 0.6$ s and $K_f = 1.11$ (see Sec. III.B)]. However, because the high bandwidth of this signal would cause crossover regression in *both* tasks in the current experiment, it was decided to also repeat the complete experiment with a second set of forcing-function signals.

Based on the findings of McRuer et al. [20,21], it was hypothesized that crossover regression could be avoided by reducing the power of the forcing function at the higher frequencies. A spectrum similar to the lowest bandwidth signal of McRuer and Jex [21], without crossover regression effects, was used for the second forcing-function signal, f_2. The amplitude distribution of this second forcing function is shown in Fig. 8a, together with the low-pass filter shaped distribution of f_1. The sinusoid frequencies ω_i and phase distribution $\phi_f(\omega_i)$ were the same for f_1 and f_2. Both amplitude distributions yield an rms of 1.875 deg.

The effect of the decreased high-frequency amplitudes in this second forcing-function spectrum is clearly visible in the time histories of Fig. 8b. Performing this experiment with both the forcing-function signals f_1 and f_2 was thought to yield a body of experimental data that could be compared with both the target-following and disturbance-rejection tasks performed by Hosman and Van der Vaart [7–9] (i.e., relatively easy and relatively difficult tracking tasks). This would also allow for investigating the effects of

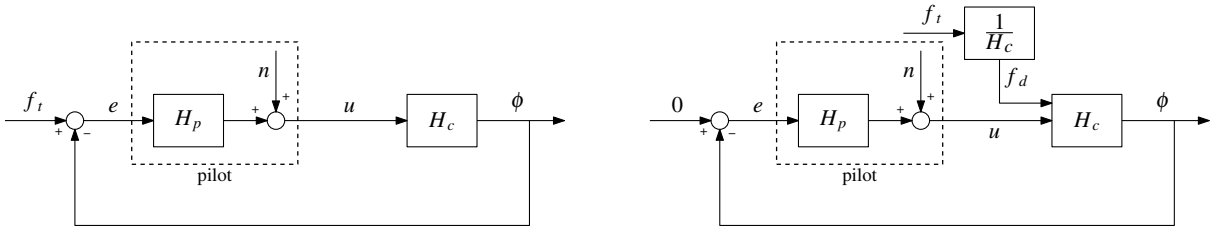

a) Target-following task b) Prefiltered disturbance-rejection task

Fig. 7 Target-following and compensated disturbance-rejection tasks of equal difficulty.

**The disturbance forcing function was not compensated for the 180-deg phase shift introduced by the double-integrator dynamics, because this phase shift does not affect task difficulty.

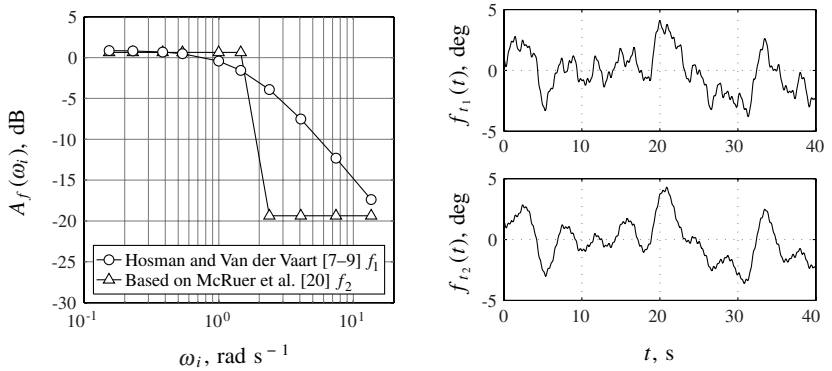

a) Amplitude distributions **b) Time histories**

Fig. 8 Experiment forcing-function signal spectra and time histories.

task bandwidth on the effectiveness of peripheral visual and physical motion cues.

In the remainder of this paper, target forcing-function signals generated according to Eq. (3) with both spectra in Fig. 8a will be indicated with a subscript t (e.g., the forcing function that was used by Hosman and Van der Vaart [7–9] will be referred to as f_{t_1}). Corresponding disturbance signals will be indicated with a subscript d (see Table 1). In addition, as was also done for the spectra in Fig. 8a, measurement data obtained with the two different forcing functions will be presented using circles and triangles, respectively.

D. Subjects and Procedure

Five subjects participated in the experiment. Their experience in manual control tasks was not as homogeneous as in the original experiment: experience ranged from "pilot-equivalent" to "experienced with laboratory tracking tasks." It was hypothesized that because the experiment mainly involves the evaluation of "universal" human perception effects on manual control behavior, any subject with good manual tracking skills would also yield valid data. For part of the experimental results, this hypothesis can be verified by comparison with those obtained by Hosman and Van der Vaart [7–9] with real pilots for exactly the same tasks.

First the original Hosman and Van der Vaart [7–9] experiment was conducted, then the experimental runs with the new forcing-function signals. Experimental conditions were gathered in sets of eight runs: target-following and disturbance-rejection tasks and four motion cue variations for each. Within each set of eight runs, the order of presentation was random.

Extensive training of subjects was performed before collecting the measurement data: the number of replications performed by each subject of each individual condition varied from 8 to 10, depending on how rapidly a stable level of tracking performance was reached. The final five runs performed by each subject for each of the eight conditions were used as the experimental measurement data.

V. Results

Measures of tracking performance, control activity, and control behavior were calculated from the experimental data. The effects of peripheral visual and physical motion cues on these properties were evaluated and the data obtained with both forcing-function signals was compared to investigate possible effects of task difficulty. The results were also compared with the original data of Hosman and Van der Vaart [7–9].

Statistical effects were analyzed using a three-factor repeated measures analysis of variance (ANOVA). The effects of the addition of peripheral P visual and physical motion M cues on the dependent measures were investigated, as well as the influence of the different forcing-function signals (FS), indicated with the factor FS in the ANOVA results. The results are summarized in Tables 2 and 3.

Table 1 Summary of experiment forcing-function signals

Forcing function	Spectrum $A_f(\omega_i)$	Forcing function	Description
f_1	Hosman and Van der Vaart [7–9]	f_{t_1}[a]	Target signal, Eq. (3)
		f_{d_1}	Disturbance signal, compensated for $H_c(j\omega)$, Eq. (4)
f_2	Based on McRuer et al. [20]	f_{t_2}	Target signal, Eq. (3)
		f_{d_2}	Disturbance signal, compensated for $H_c(j\omega)$, Eq. (4)

[a]Used by Hosman and Van der Vaart [7–9] for *both* their target-following and disturbance-rejection tasks.

Table 2 Results of repeated measures ANOVA for measured performance[a]

Independent variables		Dependent measures											
		rms e				rms u				$r_{e,u}$			
		Target		Disturbance		Target		Disturbance		Target		Disturbance	
Factor	df	F	Sig.	F	Sig.	F	Sig.	F	Sig.	F	Sig.	F	Sig.
FS	1(4)	362.3	**	89.4	**	4.9	——	9.2	*	1.6	——	1.7	——
P	1(4)	30.9	**	4.4	——	9.4	*	1.0	——	0.2	——	3.7	——
M	1(4)	54.3	**	169.4	**	4.6	——	1.6	——	0.0	——	13.0	*
FS × P	1(4)	10.7	*	0.0	——	4.0	——	1.7	——	2.0	——	0.1	——
FS × M	1(4)	46.1	**	3.3	——	0.0	——	8.3	*	0.1	——	2.2	——
P × M	1(4)	111.2	**	5.6	——	38.6	**	1.9	——	9.1	*	2.5	——
FS × P × M	1(4)	6.6	——	0.0	——	0.0	——	19.6	*	1.7	——	0.2	——

[a]Symbol definitions are as follows: ** is highly significant ($p < 0.01$), * is significant ($0.01 \leq p < 0.05$), and —— is not significant ($p \geq 0.05$).

A. Tracking Performance and Control Activity

Measured error and control signal rms values were used as indicators of tracking performance and control activity. To evaluate the relative amount of control effort required to achieve increased tracking performance, the ratio of the error and control rms values was also considered: $r_{e,u} = \text{rms}\, e / \text{rms}\, u$.

In Fig. 9, the average measured values of the three dependent measures are depicted as a function of the independent variable: the variation in motion cue availability. For each measurement condition, the five replications of all five subjects were averaged. Variance bars indicate the 95% confidence interval of the mean. The data obtained with both experimental forcing-function signals are shown separately for both types of tracking task. The original data of Hosman and Van der Vaart [7–9] are shown in gray.

Target-following and disturbance-rejection tasks of equal difficulty, being equivalent for the condition with only a compensatory display, would yield equal tracking performance and control activity. As can be verified from Fig. 9, only slight differences in error and control rms are indeed observed between target following and disturbance rejection for this condition.

1. *Error RMS*

In Figs. 9a and 9b the measured error signal rms values for both target-following and disturbance-rejection tasks are presented and compared with the measurements of Hosman and Van der Vaart [7–9], shown in gray. First of all, note the almost-perfect correspondence of the target-following error rms data obtained with f_{t_1} to those measured by Hosman and Van der Vaart [7–9]. Apparently, the effect of using nonpilots in the present experiment is minor.

Effects of peripheral visual and physical motion cues on error rms are equivalent to those observed by Hosman and Van der Vaart [7–9]. In target following, both types of motion cues improve performance; the addition of peripheral visual cues when physical motion cues are available only yields a modest performance benefit. Table 2 indicates that all effects of peripheral visual and physical motion cues and their interactions on target-following performance are indeed statistically significant. In disturbance rejection, the error rms is significantly reduced when physical motion cues are made available. The effect of peripheral visual cues on disturbance-rejection performance is small and not statistically significant.

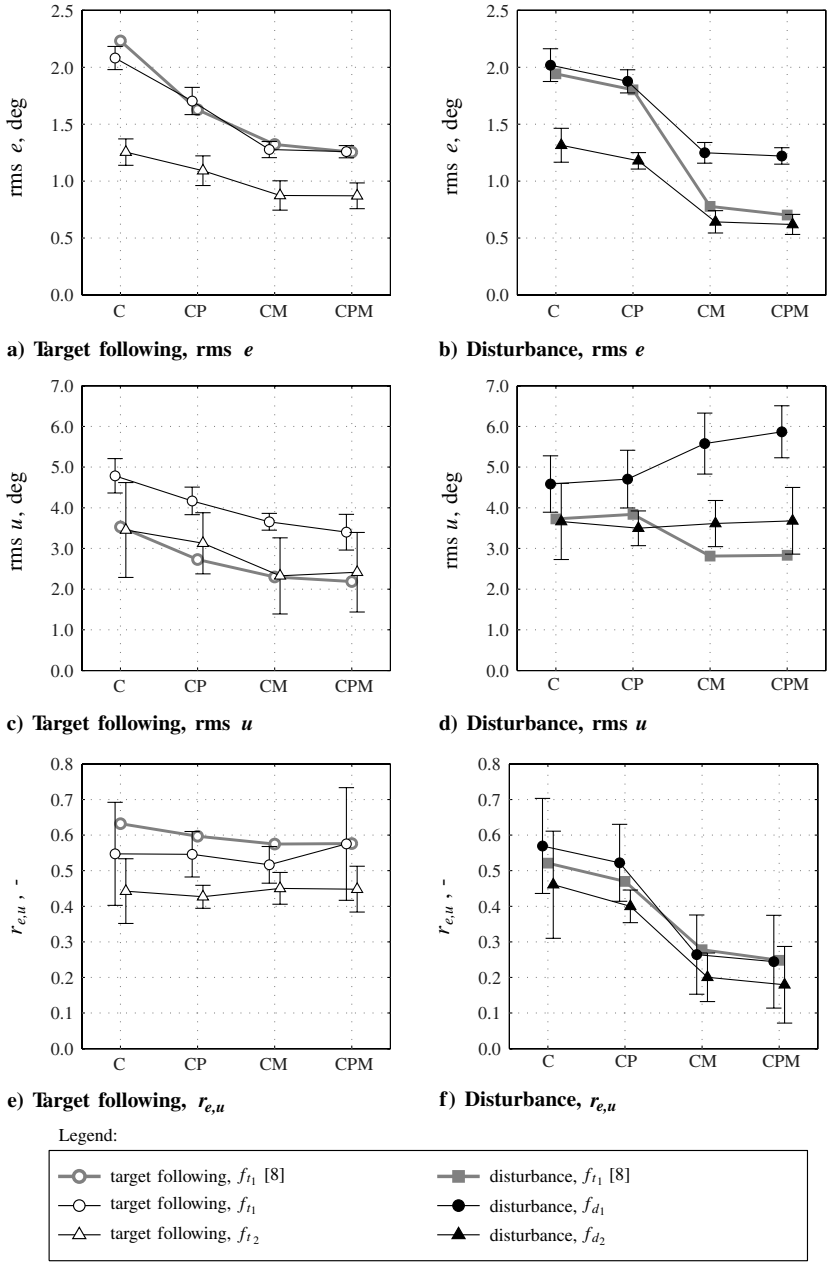

Fig. 9 Average performance and control activity for target following and disturbance rejection (all subjects).

As expected, performance for tasks performed with the easier reduced-bandwidth forcing-function signal f_2 was significantly higher than for the equivalent conditions performed with f_1. This effect holds for both types of task (see Table 2). Effects of peripheral visual and physical motion cues, however, are similar for both forcing-function signals, although for target following, a comparatively reduced performance increase is observed with f_2. This is a significant effect, judging from the ANOVA results for the interactions FS × P and FS × M for target-following error rms in Table 2. For disturbance rejection, this effect is absent.

2. Control RMS

Measured averages of the rms of the control signal u are presented in Figs. 9c and 9d for target-following and disturbance-rejection tasks, respectively. Figure 9c clearly indicates that for both target-following tasks performed with f_{t_1} and f_{t_2}, control activity decreases when extra motion cues are available, as was also found by Hosman and Van der Vaart [7–9].

Despite the clear offset between the data for f_{t_1} and f_{t_2}, the effect of forcing-function bandwidth on target-following control activity did not yield a statistically significant result because of the large spread in the data, especially for f_{t_2}. Furthermore, note that despite the good correspondence with the error rms data measured by Hosman and Van der Vaart [7–9] for a target-following task with f_{t_1}, there is quite a difference in the baseline control activity between the two sets of experimental data. This offset is thought to be the result of the fact that some of the subjects in the current experiment controlled with a relatively high gain, whereas others adopted a relatively low-gain control strategy. The trends caused by presenting peripheral visual and physical cues were found to be highly similar for both, however.

Similar to the target-following-task control activity, Hosman and Van der Vaart [7–9] measured a clear decrease in rms u when physical motion cues were available for disturbance rejection (see the gray data in Fig. 9d). Note that in the current experiment with f_{d_1}, an increase in control rms is observed for conditions with extra peripheral or physical motion cues. A nearly constant control rms for all four conditions was observed for the tasks performed with reduced forcing-function bandwidth f_{d_2}. These effects of forcing-function bandwidth are statistically significant (factor FS and its interactions with P and M in Table 2).

Note that one subject was asked to perform a number of runs of the exact disturbance-rejection task of Hosman and Van der Vaart [7–9] (i.e., with f_{t_1} as the disturbance signal). The data confirm the marked reduction in control rms for conditions CM and CPM measured by Hosman and Van der Vaart (see Fig. 10). Hence, the effects of peripheral visual and physical motion cues on control activity in disturbance rejection clearly depend on task difficulty.

3. Relative Control Effort

The data for the ratio of the error and control rms $r_{e,u}$ are shown in Figs. 9e and 9f. In target following, this ratio is found to be independent of added peripheral and physical motion cues because of the highly similar trends found in the rms values of e and u.

For all three sets of disturbance-rejection-task data shown in Fig. 9d, markedly different changes in rms u were observed with added motion cues. Despite these significant differences, the changes in $r_{e,u}$ for the addition of physical motion cues are highly similar for the three different disturbance tasks, as can be verified from Fig. 9f. A statistically significant reduction in $r_{e,u}$ (see Table 2) is observed with added physical motion cues, a reduction that does not depend on disturbance-rejection-task bandwidth.

B. Control Behavior

Linear pilot describing functions were used to evaluate the effects of peripheral visual and physical motion cues on pilot control behavior. For both target-following and disturbance-rejection tasks, the linear portion of the subjects' control actions was found to dominate all nonlinear contributions. The correlation coefficient as defined by McRuer et al. [20] was used as a measure of the linearity of pilot control behavior: $\rho^2 = 1 - S_{nn}(j\omega)/S_{uu}(j\omega)$. Figure 11 shows measured values of ρ^2 for both target following and disturbance rejection, which were generally found to be very close to one for the higher frequencies and in the crossover region.

Recently, a novel method for estimating pilot describing functions, which applies identification of linear autoregressive models with exogenous (ARX) inputs to this problem, has been developed [24]. Because it was found to be superior to conventional methods (based on the use of Fourier coefficients [25]) all frequency response functions presented here were obtained using the new method. Although the ARX method yields *continuous* frequency response function estimates, for the sake of comparing the data with the Hosman and Van der Vaart [7–9] experiment, the forcing-function signal frequencies are indicated with circles in all graphs.

1. Equivalent Pilot Describing Functions

In Fig. 12, typical pilot describing functions $H_p(j\omega)$ are depicted, representing the averaged frequency responses for one subject, obtained with forcing function f_1. Despite clear differences in control behavior between subjects, the relative effects of peripheral and physical motion cues on the measured $H_p(j\omega)$ were found to be nearly identical for all subjects and both forcing-function signals.

As was also found by Hosman and Van der Vaart [7–9], the addition of peripheral visual and physical motion cues in target following is seen to cause a reduction in equivalent pilot gain $|H_p(j\omega)|$ and a considerable increase in low-frequency phase lead, as can be verified from Figs. 12a and 12c. Such effects have also been reported in earlier experiments [5,6].

The disturbance-task magnitude responses in Fig. 12b show a clear increase due to the addition of peripheral and physical motion cues. Also, a reduction in high-frequency phase lag is observed when physical motion cues are available, indicative of a reduction in pilot time delay. Similar findings are reported by Hosman and Van der Vaart [7–9] (Fig. 4) and Levison and Junker [5], for example, who also considered a disturbance-rejection task.

Figure 12 also clearly shows that for the condition with only central visual cues (C, the white circles), the magnitude and phase responses are now equivalent for both target-following and disturbance-rejection tasks. This is further proof that the discrepancy in task difficulty, which caused differences in control behavior in the Hosman and Van der Vaart [7–9] experiment, was compensated for successfully. Despite the fact that the disturbance-rejection task performed in the current experiment had significantly more high-frequency signal content, the effects of peripheral visual and physical motion cues on measured pilot describing functions were found to be similar to those reported by Hosman and Van der Vaart.

In general, the results of the current experiment with respect to the effects of peripheral visual and physical motion cues on pilot control behavior (for all subjects and both experiment forcing-function signals) agree with those of Hosman and Van der Vaart [7–9].

2. Crossover Frequency, Phase Margin, and Pilot Time Delay

The crossover frequency and phase margin were calculated from measured pilot describing functions $H_p(j\omega)$. Corresponding

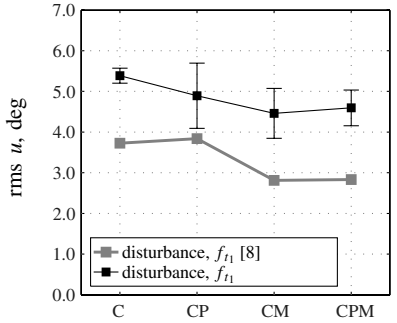

Fig. 10 Control activity for Van der Vaart [8] disturbance task (subject 3, average and standard deviation of 3 runs).

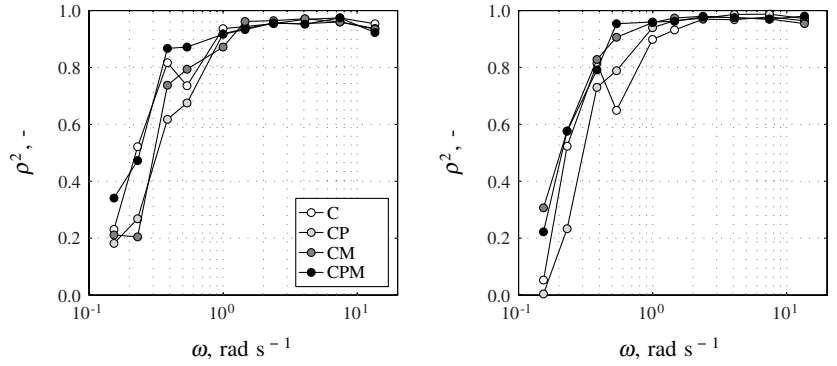

a) Target following **b) Disturbance**

Fig. 11 Average ρ^2 correlation coefficients at forcing-function frequencies (subject 1, f_1).

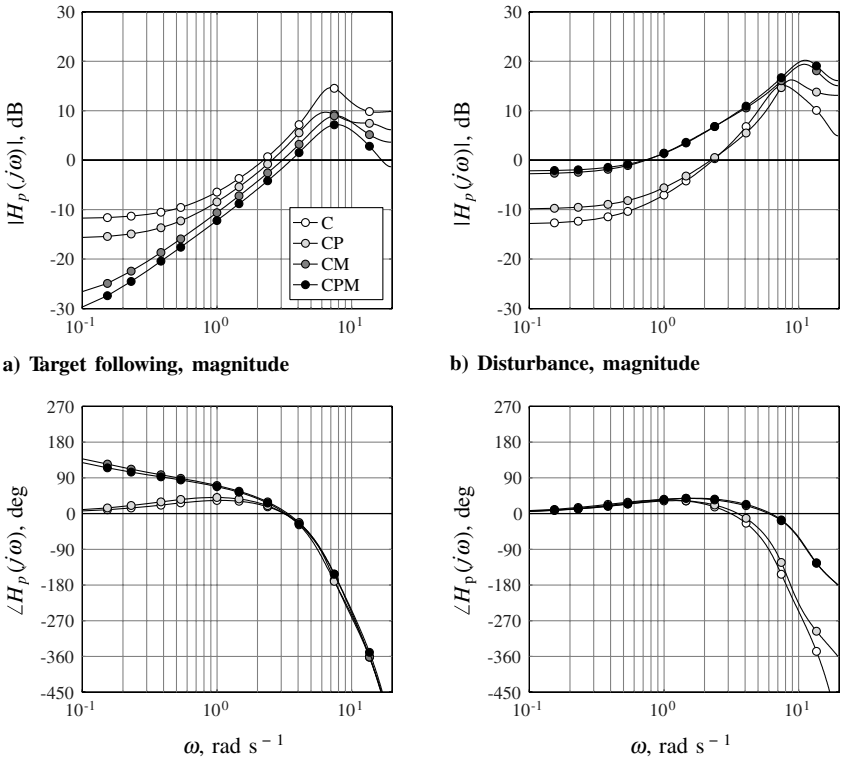

a) Target following, magnitude **b) Disturbance, magnitude**

c) Target following, phase **d) Disturbance, phase**

Fig. 12 Representative target-following and disturbance-rejection-task pilot describing functions (subject 1, f_1).

effective pilot time delays were calculated from ω_c and φ_m using the relation between these parameters defined for the crossover model [21]: $\varphi_m = \pi/2 - \omega_c \tau_e$. The measured crossover frequencies, phase margins, and pilot effective time delays are depicted in Fig. 13, together with the data reported by Van der Vaart [8], shown in gray. Results for target following and disturbance rejection are shown side by side for these three parameters; variance bars again indicate 95% confidence intervals. Table 3 summarizes the results of a repeated measures ANOVA.

Figures 13a and 13b show that all data are approximately the same for the conditions with only the compensatory visual display. The changes in crossover frequency ω_c with added peripheral and physical cues are similar to those observed for the magnitude of $H_p(j\omega)$: a decrease for target-following tasks and a marked increase for disturbance-rejection tasks. The addition of peripheral visual cues is only significant for the disturbance tasks. These effects confirm the results found by Hosman and Van der Vaart [7–9].

A clear effect of forcing-function bandwidth on target-following-task crossover frequency is observed: significantly higher crossover frequencies were found for target-following tasks performed with the lower-bandwidth forcing function f_{t_2}. This effect was very consistent over the measurement data, as indicated by the highly significant effect of the factor FS (Table 3). For disturbance rejection, no significant effect of task bandwidth on ω_c was found. The measured crossover frequencies were clearly lower, however, than those obtained by Hosman and Van der Vaart [7–9] (see Fig. 13b).

Figure 13c and Table 3 reveal that the addition of peripheral or physical motion cues yields a significant increase in target-following-task phase margin φ_m, to over 70 deg for f_1. In disturbance rejection, the phase margin remains approximately constant when extra motion cues are made available, which can be verified from Fig. 13d and Table 3. A significant reduction in phase margin is found with reduced forcing-function bandwidth for both target-following ($F_{1,4} = 45.176$ and $p = 0.003$) and disturbance-rejection tasks ($F_{1,4} = 9.628$ and $p = 0.036$).

Although these different trends in phase margin that result from the addition of peripheral visual and physical motion cues are regarded as representative for both tasks, they are at least partly

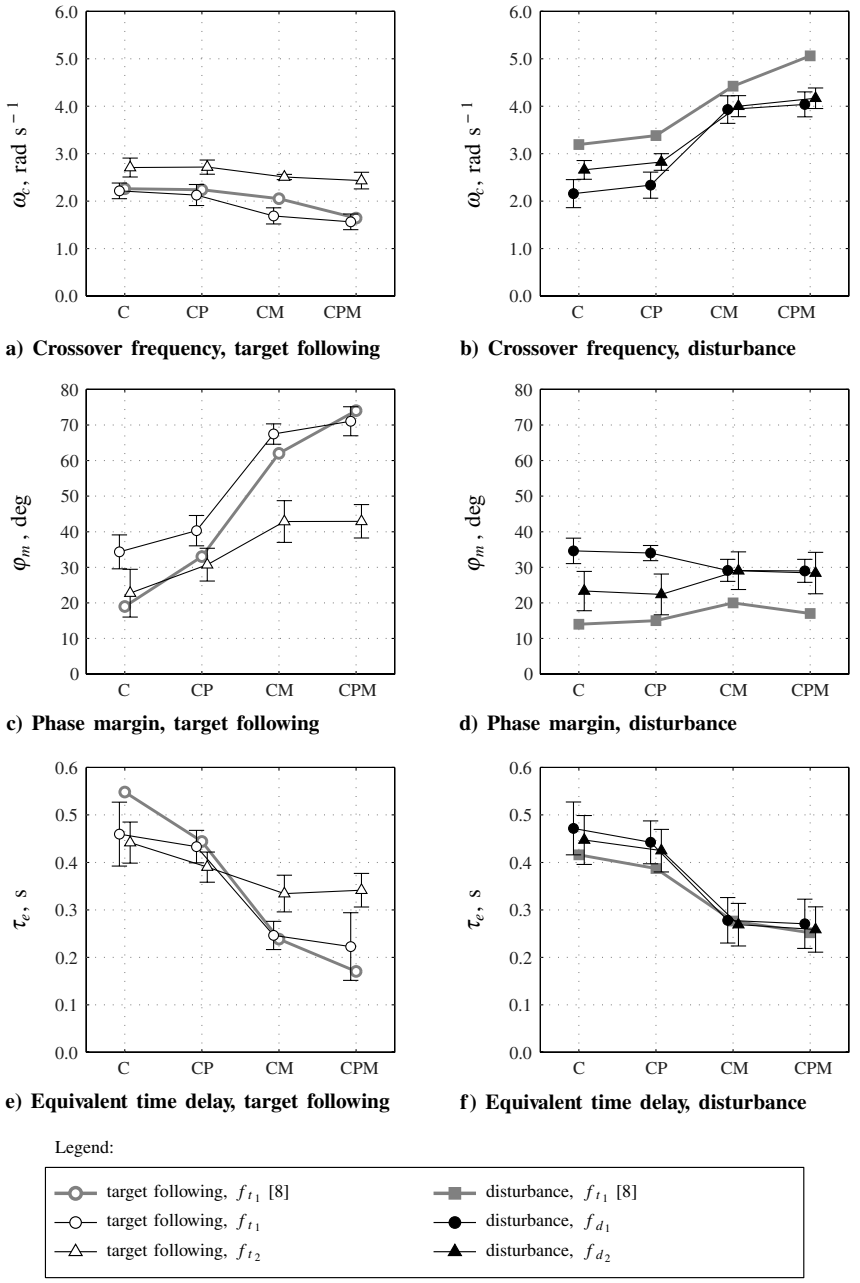

Fig. 13 Average crossover frequency, phase margin and pilot time delay (all subjects).

caused by the different control-theoretic structures of the equivalent pilot describing function $H_p(j\omega)$, as already mentioned in Sec. III.B. This is illustrated in Fig. 14, in which changes in crossover frequency and phase margin as a function of the magnitude of $H_{p_\phi}(j\omega)$ are depicted for both target following and disturbance rejection. For this simplified example, it was assumed that $H_{p_\phi}(j\omega) = K_{p_\phi} j\omega$, which is a reasonable simplification of the pilot's response to ϕ for control of double-integrator dynamics. For the response to the tracking error

Table 3 Results of repeated measures ANOVA on measured crossover parameters[a]

Independent variables		Dependent measures											
		ω_e				φ_m				τ_e			
		Target		Disturbance		Target		Disturbance		Target		Disturbance	
Factor	df	F	Sig.	F	Sig.	F	Sig.	F	Sig.	F	Sig.	F	Sig.
FS	1(4)	67.0	**	1.6	——	45.2	**	9.6	*	2.1	——	0.4	——
P	1(4)	1.9	——	41.1	**	9.2	*	1.5	——	6.8	——	7.3	——
M	1(4)	20.3	*	152.9	**	151.0	**	0.0	——	34.4	**	38.4	**
FS × P	1(4)	1.2	——	0.1	——	0.1	——	0.4	——	0.0	——	0.1	——
FS × M	1(4)	23.2	**	3.1	——	23.9	**	4.3	——	19.9	*	0.1	——
P × M	1(4)	0.5	——	0.3	——	5.7	——	2.1	——	12.7	*	13.8	*
FS × P × M	1(4)	0.2	——	1.0	——	3.6	——	0.0	——	8.9	*	0.6	——

[a]Symbol definitions are as follows: ** is highly significant ($p < 0.01$), * is significant ($0.01 \leq p < 0.05$), and —— is not significant ($p \geq 0.05$).

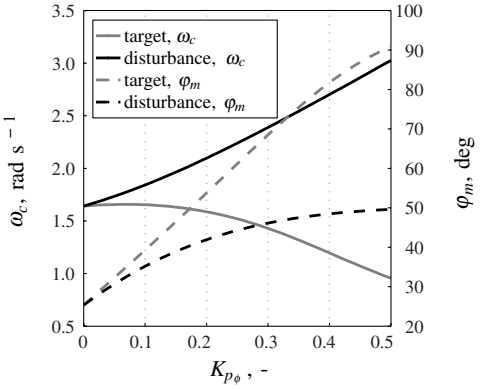

Fig. 14 Variations in crossover frequency and phase margin for increasing values of the gain of $H_{p_\phi}(j\omega)$.

$H_{p_e}(j\omega)$, a model identified in data from the Hosman and Van der Vaart [7–9] experiment was selected [8], which was kept fixed for investigating the effect of varying K_{p_ϕ}. Note from Fig. 14 that disturbance-rejection crossover frequency increases with increasing values of K_{p_ϕ}, whereas it decreases for target following. Also, the increase in phase margin is much larger for target following than for disturbance rejection. The differences in crossover frequency and phase margin between target following and disturbance rejection observed in Fig. 13 should be interpreted with this in mind.

In both target following and disturbance rejection, the addition of peripheral visual and physical motion cues leads to a reduction in the equivalent time delay τ_e (Figs. 13e and 13f). This reduction is of the same magnitude for both tasks and statistically significant for added physical motion cues only (Table 3). No significant effect of the FS is observed on the equivalent time delay for both target following and disturbance rejection, ($F_{1,4} = 2.101$ and $p = 0.221$) and ($F_{1,4} = 0.432$ and $p = 0.551$), respectively.

For all three parameters shown in Fig. 13, a significant effect of the interaction of physical motion cues and forcing-function signal FS × M (Table 3) exists for target following. The reduction of ω_c and τ_e and the increase in φ_m caused by physical motion cues are clearly smaller in target following with f_{t_2} than measured with the original forcing function f_{t_1}. A significant effect of this interaction was also observed in the measured error rms data, in which a reduction in task bandwidth also caused a reduced relative performance increase. This suggests that the effectiveness of motion cues in target-following tasks depends on the difficulty of the task and that for very low-bandwidth target-following tasks there may not be any effect at all. The effectiveness of motion cues in disturbance rejection, however, appears to be independent of task bandwidth: the effects of extra motion cues on performance and control behavior are of similar magnitude for both disturbance-rejection tasks performed in this experiment *and* the low-bandwidth task performed by Hosman and Van der Vaart [7–9].

VI. Frequency-Domain Analysis

Even though the effects are not of equal magnitude, the addition of both peripheral visual and physical motion cues in roll-attitude tracking with double-integrator dynamics was found to yield increased performance. Since the research performed into the relation between tracking performance and control behavior by McRuer et al. [20], an increased crossover frequency is generally associated with such enhanced tracking performance. For compensatory disturbance rejection (for which additional motion cues allow for parallel perception of the tracking error), this reasoning clearly holds, because a significant increase in both performance and crossover frequency is observed when peripheral visual and physical motion cues are made available.

For target following, a similar performance increase is observed. From the analysis of the corresponding control behavior, however, no increase in crossover frequency was found. Instead, the phase margin is found to increase significantly, whereas ω_c decreases slightly. Increased tracking performance due to the addition of extra motion cues is apparently associated with different changes in equivalent pilot response $H_p(j\omega)$ for compensatory target following and disturbance rejection, which is at least partly a result of the *different* function of these extra cues in both tasks. This will be investigated in this section by evaluating increased performance in terms of closed-loop attenuation of tracking errors in the frequency domain.

A. Closed-Loop Attenuation of Tracking Errors

The effectiveness of the closed-loop control system, of which the pilot is an integral part, in suppressing error can be evaluated by investigating how the forcing-function signals are translated into the error signal e. Using both compensatory task structures in Fig. 1, which with the definitions of $H_p(j\omega)$ of Eqs. (1) and (2) also hold for tasks with additional peripheral and physical cues, the following frequency-domain relations can be derived:

$$H_{e,f_t}(j\omega) = \frac{E(j\omega)}{F_t(j\omega)} = \frac{1}{1 + H_p(j\omega)H_c(j\omega)} \tag{5}$$

$$H_{e,f_d}(j\omega) = \frac{E(j\omega)}{F_d(j\omega)} = \frac{-H_c(j\omega)}{1 + H_p(j\omega)H_c(j\omega)} \tag{6}$$

Figures 15a and 15b show the absolute value of these relations , using the measured frequency response functions $H_p(j\omega)$ for target-following and disturbance-rejection tasks.

The boundary between amplification and attenuation of tracking errors introduced by the forcing functions f_t and f_d is the case in which the magnitude of $H_{e,f_t}(j\omega)$ and $H_{e,f_d}(j\omega)$ are equal to 0 dB. Tracking errors are attenuated at a specific frequency ω_i if the absolute value of its closed-loop relation with the tracking error e, as described by Eqs. (5) and (6), is smaller than unity [i.e.,

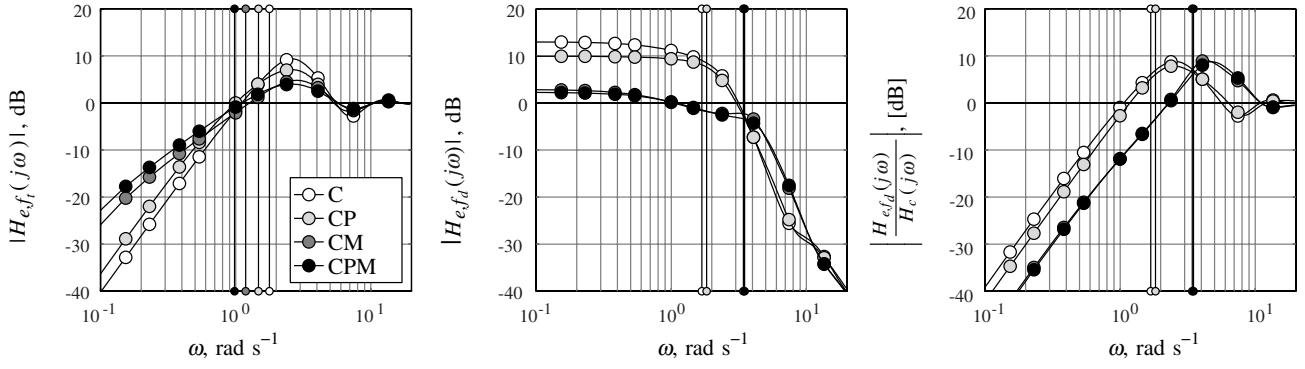

a) Target following **b) Disturbance** **c) Disturbance**

Fig. 15 Measured closed-loop error frequency response functions (subject 1, f_1).

$|H_{e,f_t}(j\omega_i)| < 1$ or $|H_{e,f_d}(j\omega_i)| < 1$]. From Fig. 15, it is clear that this requirement for error attenuation is not met at all forcing-function frequencies: for both tasks, the measured error frequency responses are found to be above 0 dB in certain frequency ranges.

For target-following tasks (Fig. 15a), the main amplification of closed-loop error occurs just above the crossover frequency, indicated with the vertical lines for each condition: a significant peak in $|H_{e,f_t}(j\omega)|$ is observed at frequencies between 2 and 3 rad/s. The effect of adding motion cues is to lower the magnitude of this peak, which in control-theoretic terms corresponds with increased closed-loop stability and increased tracking performance.

The main amplification of forcing-function errors in disturbance rejection occurs in the *lower* frequency range (Fig. 15b). The addition of physical motion, in particular, clearly reduces the low-frequency error amplification, yielding better tracking performance. Here, improved disturbance suppression is achieved by increasing the loop gain.

Despite the fact that Fig. 15b correctly reflects closed-loop error attenuation in disturbance rejection, this relation between disturbance signal f_d and tracking error e is never observable for the human pilot, due to the fact that f_d first travels through the system dynamics $H_c(j\omega)$; only its filtered equivalent $F_d(j\omega)H_c(j\omega)$ is observable. Therefore, from a pilot-centered perspective, it is more correct to investigate error attenuation of the effective target signal caused by the disturbance forcing function: $H_{e,f_d}(j\omega)/H_c(j\omega)$, illustrated in Fig. 15c. Figures 15a and 15c clearly reflect the observed changes in ω_c and φ_m measured for both target following and disturbance rejection, respectively.

B. Attenuation of Tracking Errors in Target-Following Tasks

Van der Vaart [8] used the error transfer functions (5) and (6) to derive theoretical limits on the equivalent pilot describing function $H_p(j\omega)$ that would ensure error reduction at ranges of forcing-function frequencies. Evaluation of $|H_{e,f_t}(j\omega_i)| < 1$ yields

$$|1 + H_p(j\omega)H_c(j\omega)| = |1 + H_{\text{ol}}(j\omega)| > 1 \tag{7}$$

The requirement for error attenuation of Eq. (7) can be evaluated by observing the Nyquist locus of the open-loop response, as shown in Fig. 16. The area in which the condition of Eq. (7) is not met (i.e., in which tracking errors are amplified) is depicted by the dark-gray-shaded circle with its center at the -1 point in the Nyquist plane.

The crossover frequency of the Nyquist loci is defined as their intersection with the origin-centered unit circle (the dashed black circle), in which the open-loop magnitude equals 1. For frequencies around and, especially, above crossover, the open-loop response is inside the error amplification area for all conditions. This is the frequency range in which the magnitude of the closed-loop error response in Fig. 15a is above 0 dB.

The error-attenuation requirement of Eq. (7) is defined in terms of the open-loop response $H_{\text{ol}}(j\omega)$. Translation of this limit to requirements on the pilot response $H_p(j\omega)$ is not straightforward. A conservative approximation (which is only valid for frequencies well below ω_c, in which the loci are far away from the origin) can be obtained (here, with double-integrator dynamics), by rewriting Eq. (7) in terms of $H_p(j\omega)$ [8]:

$$|H_p(j\omega_i)| > \frac{2\omega_i^2}{K_c}, \qquad \omega_i \ll \omega_c \tag{8}$$

This approximation (the larger light-gray-shaded circle in Fig. 16) is valid for the Nyquist loci corresponding to conditions without physical motion cues (C and CP), because the edges of both circles are close together in the quadrant from which the loci approach the origin for increasing frequencies. Measured data for conditions CM and CPM indicate that subjects ensured error attenuation at frequencies around crossover by increasing their phase lead instead of attempting to satisfy Eq. (8). Equivalent pilot phase $\angle H_p(j\omega)$ can be read from Fig. 16 as the counterclockwise angle of a point on the Nyquist locus with respect to the negative real axis. Error amplification is avoided at frequencies around crossover if

$$\angle H_p(j\omega_i) > 60\,\text{deg}, \qquad \omega_i \le \omega_c \tag{9}$$

In Fig. 17, the lower bounds on pilot magnitude [Eq. (8)] and phase [Eq. (9)] are depicted with measured target-following frequency response functions. Clearly, the increase in low-to-midfrequency pilot phase $\angle H_p(j\omega)$ due to presenting physical motion cues in target-following tasks ensures error reduction at frequencies up to ω_c. Figure 16 shows that for frequencies just below crossover, Eq. (8) is violated for tasks with physical motion cues, but error attenuation is still achieved because Eq. (9) is met. Hence, an increase in pilot phase around crossover, measured as an increase in phase margin φ_m, is an effective strategy for enhancing closed-loop tracking error attenuation in target following.

C. Reduction of Tracking Errors in Disturbance-Rejection Tasks

A similar analysis holds for disturbance rejection. When $|H_{e,f_d}(j\omega_i)| < 1$, then

$$\left|H_p(j\omega_i) - \omega_i^2/K_c\right| > 1 \tag{10}$$

To reduce tracking errors at ω_i, the absolute value of the difference between $H_p(j\omega_i)$ and ω_i^2/K_c should be larger than unity. Figure 18 illustrates this limit as the gray-shaded circle, indicating that the inequality in Eq. (10) is not met. Note that the position of the center of this circle depends on the frequency that is evaluated (in this case, $\omega_i = 4.065$ rad/s): for increasing frequencies, the circle will move further along the positive real axis. The black curve in Fig. 18 indicates the Nyquist locus of a measured pilot frequency response $H_p(j\omega)$; black circles indicate forcing-function frequencies. The value of $H_p(j\omega)$ at the considered sinusoid frequency ω_i is indicated on the locus with a white circle.

Rewriting Eq. (10) as limits on the magnitude and phase of $H_p(j\omega)$ is again troublesome, but can be approximated with the four hatched boundaries depicted in Fig. 18 [8]. Upper and lower bounds on the magnitude of the pilot response $|H_p(j\omega)|$ can be defined in terms of the two origin-centered circular limits:

$$|H_p(j\omega_i)| > \omega_i^2/K_c + 1 \tag{11}$$

$$|H_p(j\omega_i)| < \omega_i^2/K_c - 1 \tag{12}$$

Pilot phase requirements follow from the linear dashed bounds:

$$|\angle H_p(j\omega_i)| > \arcsin\left(K_c/\omega_i^2\right) \tag{13}$$

If one of Eqs. (11–13) is met, error attenuation at a frequency ω_i is guaranteed. From analysis of graphs like Fig. 18 for various frequencies along the measured Nyquist loci, it was found that only one of these three limits is important for achieving error attenuation

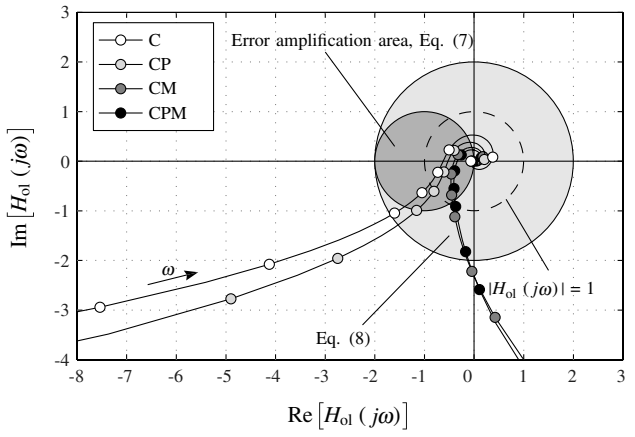

Fig. 16 Nyquist loci of measured target-following-task open-loop frequency responses (subject 1, f_1).

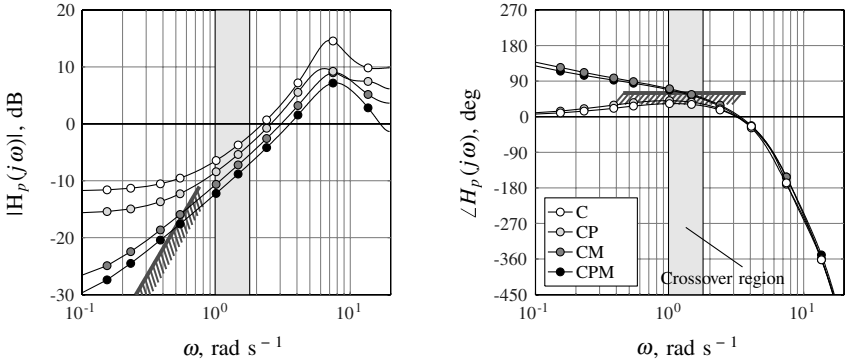

a) Magnitude b) Phase

Fig. 17 Measured target following describing functions $H_p(j\omega)$ with magnitude and phase limits defined by Eqs. (8) and (9) (subject 1, f_1).

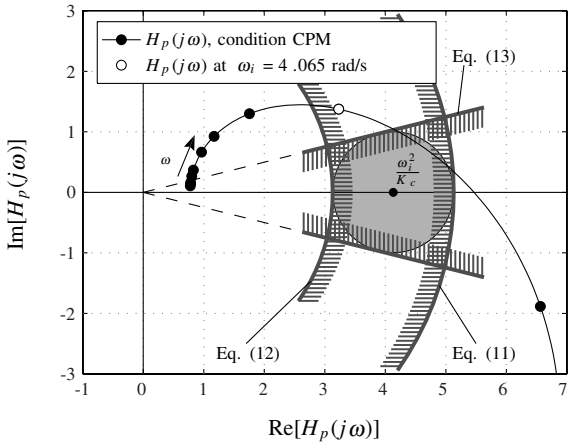

Fig. 18 Nyquist locus of measured pilot frequency response (subject 1, f_1, condition CPM) with limits defined by Eqs. (11–13) evaluated for $\omega_i = 4.065$ rad/s (white circle on locus).

in specific frequency ranges. For low frequencies ($\omega_i < \omega_c$), the lower bound on $|H_p(j\omega)|$ [Eq. (11)] is the most critical, whereas the upper bound on pilot magnitude [Eq. (12)] is applicable to higher frequencies ($\omega_i > \omega_c$). In the midfrequency range (and therefore in the crossover area), the pilot phase limits [Eq. (13)] are critical. In Fig. 19, the three limits defined by Eqs. (11–13) are depicted with measured pilot frequency response magnitudes and phases for conditions C to CPM.

Figure 19a shows that the measured pilot magnitudes move closer to the boundary defined by Eq. (11) when extra motion cues are added. For other subjects and for the lower-bandwidth forcing-function signal f_{d_2}, the magnitude of $H_p(j\omega)$ is found to move outside of the boundary for conditions with physical motion cues. This is consistent with the increased low-frequency disturbance-rejection error attenuation shown in Fig. 15b. As can also be verified from Fig. 19a, pilot response magnitudes move closer to or even cross the boundary defined by Eq. (12) for the higher frequencies.

As is clearly visible in Fig. 19b, the increase in crossover frequency measured for disturbance-rejection tasks also implies that the pilot phase lead extends to higher frequencies. This results in better compliance with the phase limit of Eq. (13) for the forcing sinusoid with its frequency just above crossover. For most other subjects, this was also found for frequencies in the crossover region.

D. Tracking Error Attenuation in the Crossover Region

The most striking observation from these derivations of limits on error attenuation is that for both target-following and disturbance-rejection tasks, the addition of physical motion cues allows for closed-loop reduction of tracking errors around crossover. More specifically, as can be judged from Figs. 17b and 19b, these cues cause the limits on pilot phase $\angle H_p(j\omega)$ to be met, which were generally violated for conditions C and CP.

Apparently, physical motion cues allow subjects to achieve effective error attenuation in the crossover region, in which these phase limits are applicable, in both types of compensatory tracking. This is even more clear from the graph shown in Fig. 20, in which measured phase margins are depicted as a function of crossover frequency. Because the limits defined by Eqs. (9) and (13) also hold at the crossover frequency ω_c, these are shown together with the measured data. Measured data from the Hosman and Van der Vaart [7–9] experiment are shown in gray.

First of all, for all of the measured target-following or disturbance-rejection tasks, the error-attenuation limits were not met for conditions C and CP. Hence, without physical motion cues, it is found to be impossible to reduce tracking errors at ω_c. When adding

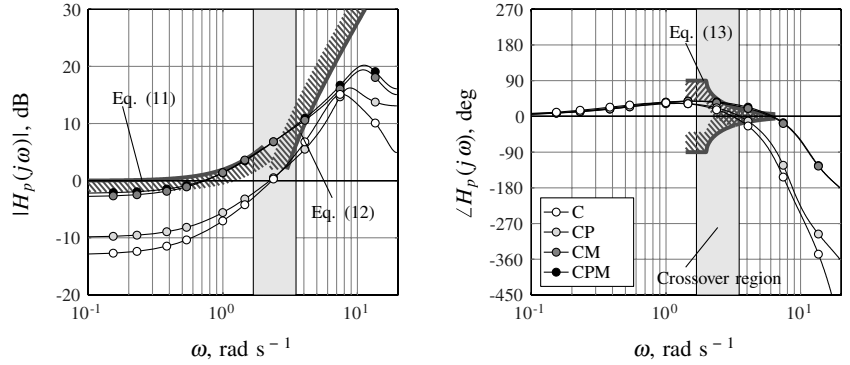

a) Magnitude b) Phase

Fig. 19 Measured disturbance-task pilot frequency response functions $H_p(j\omega)$ with magnitude and phase limits defined by Eqs. (11–13) (subject 1, f_1).

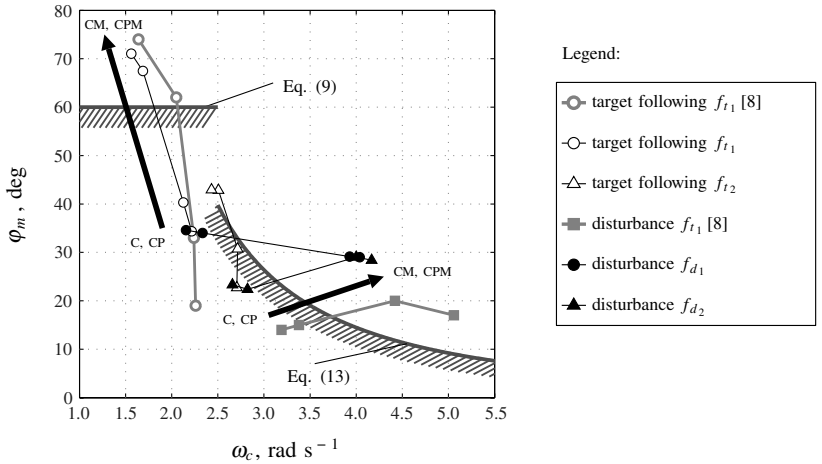

Fig. 20 Measured average phase margins as a function of crossover frequency.

peripheral visual and, especially, physical motion cues, the operating point (i.e., the combination of ω_c and φ_m) moves toward the error-attenuation boundary that holds for the particular task. For the conditions with physical motion cues, the data no longer violate the error-attenuation limits defined by Eqs. (9) and (13) for all tasks, except the low-bandwidth target-following task performed with the forcing function f_{t_2} in the current experiment.

VII. Discussion

The goal of this research was to identify effects of peripheral visual and physical motion cues on pilot tracking performance and control behavior in compensatory target-following and disturbance-rejection tasks. The results of the current experiment indicate that the discrepancy in baseline task difficulty of both types of tasks in the original Hosman and Van der Vaart [7–9] experiment has not resulted in invalidation of most of the main effects of peripheral visual and physical motion cues they have reported:

1) For both types of compensatory tracking, the addition of peripheral visual and physical motion cues yields an increase in tracking performance.

2) The effect of peripheral visual cues is more significant in target-following than in disturbance-rejection tasks.

3) The addition of peripheral visual cues when physical motion cues are already provided yields only minor improvements in performance and slight changes in control behavior.

4) For disturbance-rejection tasks, the addition of extra peripheral or physical motion cues allows for an increase in crossover frequency ω_c, whereas the phase margin is found to remain constant. Here, additional motion cues allow for a control with a relatively higher gain, without loss of stability.

5) For target-following tasks, the addition of extra motion cues results in a slight reduction in the crossover frequency and a significant increase in phase margin.

The addition of peripheral visual and physical motion cues yields a highly similar performance increase in target following and disturbance rejection. However, the underlying changes in control strategy, as indicated by measured pilot describing functions $H_p(j\omega)$ and corresponding crossover frequencies and phase margins, were found to differ significantly for both types of tasks. A control-theoretical analysis of closed-loop tracking error attenuation revealed that the distinctly different trends in control behavior that are observed when physical motion cues are made available are due to different optimal strategies for increasing tracking performance in both types of task, especially at frequencies around crossover.

Because of the use of two sets of forcing-function signals in the current experiment, some effects of forcing-function bandwidth and task difficulty on the use of peripheral visual and physical motion cues were identified. This revealed the only real deviation from the results of Hosman and Van der Vaart [7–9]: the measured effect of extra motion cues on disturbance-rejection-task control activity. Hosman and Van der Vaart found that the control signal rms values decreased in their low-bandwidth disturbance-rejection task when physical motion cues were available. In the current experiment, effects of extra motion cues in disturbance rejection were found to be highly dependent on the forcing-function bandwidth. A clear *increase* in rms u was found with the highest forcing-function bandwidth, f_1, whereas the same task performed with the reduced-bandwidth signal, f_2, showed no significant change. Performance gains caused by extra motion cues and changes in control behavior in disturbance rejection were, however, found to be independent of forcing-function bandwidth.

In target following, a reduction in forcing-function bandwidth showed a reduced magnitude of all effects of peripheral visual and physical motion cues on tracking performance and control behavior. This is especially visible in a reduced decrease in error rms and a reduced increase in phase margin φ_m, compared with measurements with f_1. These results suggest that the effectiveness of peripheral visual and physical motion cues for target following is highly dependent on task difficulty and is larger for more difficult tasks.

The target-following task evaluated in the current research was still relatively difficult due to the fact that double-integrator dynamics were controlled. For such higher-order controlled elements, physical motion cues provide especially valuable information for stabilizing the controlled system rates. As, for instance, reported by Shirley and Young [2], motion cue effects also tend to reduce when systems with relatively easier dynamics are controlled. Because aircraft dynamics are generally approximately first-order, simulator motion cues may not be significantly beneficial at all for aircraft manual control tasks that are comparable with a target-following task. This suggests that simulator motion cues might not be required for accurate representation of such tasks in flight simulation. The current research seems to indicate, however, that the benevolent effect of physical motion cues for disturbance-rejection tasks might persist even for aircraft-representative dynamics. Further research is needed to verify this hypothesis.

VIII. Conclusions

In both compensatory target-following and disturbance-rejection tasks, peripheral visual and, in particular, physical motion cues are found to increase tracking performance. Whereas in target following, the effectiveness of additional motion cues depends on task difficulty, no such effects are found for disturbance rejection. Significant differences in control behavior are observed between target following and disturbance rejection when peripheral visual and physical motion cues are made available. These differences can be explained by the different function that the peripheral visual and physical motion perceptual modes have in both tasks, because these result in different strategies for improving tracking performance.

Acknowledgments

The authors would like to thank all the subjects who performed this extensive simulator experiment. In addition, they would like to express their gratitude to the reviewers of this paper for their highly useful insights and comments.

References

[1] Meiry, J. L., "The Vestibular System and Human Dynamic Space Orientation," NASA CR-628, 1967.

[2] Shirley, R. S., and Young, L. R., "Motion Cues in Man-Vehicle Control," *IEEE Transactions on Man-Machine Systems*, Vol. 9, No. 4, Dec. 1968, pp. 121–128. doi:10.1109/TMMS.1968.300016

[3] Stapleford, R. L., Peters, R. A., and Alex, F. R., "Experiments and a Model for Pilot Dynamics with Visual and Motion Inputs," NASA CR-1325, 1969.

[4] Moriarty, T. E., Junker, A. M., and Price, D. R., "Roll Axis Tracking Improvement Resulting from Peripheral Vision Motion Cues," *Twelfth Annual Conference on Manual Control*, NASA-TM-X-73-170, NASA Ames Research Center, Moffett Field, CA, 1976, pp. 868–894.

[5] Levison, W. H., and Junker, A. M., "A Model for the Pilot's Use of Motion Cues in Roll-Axis Tracking Tasks," Bolt Beranek and Newman Inc., TR 3528, Cambridge, MA, 1977.

[6] Levison, W. H., "A Model for the Pilot's Use of Roll-Axis Motion Cues in Steady-State Tracking Tasks," Bolt Beranek and Newman Inc., TR 3808, Cambridge, MA, 1978.

[7] Hosman, R. J. A. W., and Van der Vaart, J. C., "Effects of Vestibular and Visual Motion Perception on Task Performance," *Acta Psychologica*, Vol. 48, Nos. 1–3, Jan. 1981, pp. 271–287. doi:10.1016/0001-6918(81)90067-6

[8] Van der Vaart, J. C., "Modelling of Perception and Action in Compensatory Manual Control Tasks," Ph.D. Thesis, Faculty of Aerospace Engineering, Delft Univ. of Technology, Delft, The Netherlands, 1992.

[9] Hosman, R. J. A. W., "Pilot's Perception and Control of Aircraft Motions," Ph.D. Thesis, Faculty of Aerospace Engineering, Delft Univ. of Technology, Delft, The Netherlands, 1996.

[10] Hess, R. A., "Model for Human Use of Motion Cues in Vehicular Control," *Journal of Guidance, Control, and Dynamics*, Vol. 13, No. 3, 1990, pp. 476–482.

[11] Telban, R. J., and Cardullo, F. M., "An Integrated Model of Human Motion Perception with Visual Vestibular Interaction," AIAA Modeling and Simulation Technologies Conference and Exhibit, Montreal, Canada, AIAA Paper 2001-4249, 2001.

[12] Zeyada, Y., and Hess, R. A., "Modeling Human Pilot Cue Utilization with Applications to Simulator Fidelity Assessment," *Journal of Aircraft*, Vol. 37, No. 4, 2000, pp. 588–597.

[13] Hess, R. A., and Siwakosit, W., "Assessment of Flight Simulator Fidelity in Multiaxis Tasks Including Visual Cue Quality," *Journal of Aircraft*, Vol. 38, No. 4, 2001, pp. 607–614.

[14] Hosman, R. J. A. W., "Are Criteria for Motion Cueing and Time Delays Possible?," AIAA Modeling and Simulation Technologies Conference and Exhibit, Portland, OR, AIAA Paper 1999-4028, 1999.

[15] Dehouck, T. L., Mulder, M., and Van Paassen, M. M., "The Effects of Simulator Motion Filter Settings on Pilot Manual Control Behaviour," AIAA Modeling and Simulation Technologies Conference and Exhibit, Keystone, CO, AIAA Paper 2006-6250, 2006.

[16] Hosman, R. J. A. W., and Van der Vaart, J. C., "Visual-Vestibular Interaction in Pilot's Perception of Aircraft or Simulator Motion," AIAA Modeling and Simulation Technologies Conference, Atlanta, GA, AIAA Paper 1988-4622, 1988.

[17] Kaljouw, W. J., Mulder, M., and Van Paassen, M. M., "Multi-Loop Identification of Pilot's Use of Central and Peripheral Visual Cues," AIAA Modeling and Simulation Technologies Conference and Exhibit, Providence, RI, AIAA Paper 2004-5443, 2004.

[18] Löhner, C., Mulder, M., and Van Paassen, M. M., "Multi-loop Identification of Pilot Central Visual and Vestibular Motion Perception Processes," Proceedings of the AIAA Modeling and Simulation Technologies Conference and Exhibit, San Francisco, AIAA Paper 2005-6503, 2005.

[19] Duppen, M., Zaal, P. M. T., Mulder, M., and Van Paassen, M. M., "Effects of Motion on Pilot Behavior in Target, Disturbance and Combined Tracking Tasks," AIAA Modeling and Simulation Technologies Conference and Exhibit, Hilton Head, SC, AIAA Paper 2007-6894, 2007.

[20] McRuer, D. T., Graham, D., Krendel, E., and Reisener, W., "Human Pilot Dynamics in Compensatory Systems. Theory, Models and Experiments with Controlled Element and Forcing Function Variations," U.S. Air Force Flight Dynamics Lab., TR AFFDL-TR-65-16, Wright–Patterson AFB, OH, 1965.

[21] McRuer, D. T., and Jex, H. R., "A Review of Quasi-Linear Pilot Models," *IEEE Transactions on Human Factors in Electronics*, Vol. HFE-8, No. 3, 1967, pp. 231–249. doi:10.1109/THFE.1967.234304

[22] Stroosma, O., Van Paassen, M. M., Mulder, M., and Postema, F., "Measuring Time Delays in Simulator Displays," AIAA Modeling and Simulation Technologies Conference and Exhibit, Hilton Head, SC, AIAA Paper 2007-6562, 2007.

[23] Berkouwer, W. R., Stroosma, O., Van Paassen, M. M., Mulder, M., and Mulder, J. A., "Measuring the Performance of the SIMONA Research Simulator's Motion System," AIAA Modeling and Simulation Technologies Conference and Exhibit, San Francisco, AIAA Paper 2005-6504, 2005.

[24] Nieuwenhuizen, F. M., Zaal, P. M. T., Mulder, M., Van Paassen, M. M., and Mulder, J. A., "Modeling Human Multi-Channel Motion Perception and Control Using Linear Time-Invariant Models," *Journal of Guidance, Control, and Dynamics* (accepted for publication).

[25] Van Paassen, M. M., and Mulder, M., "Identification of Human Control Behavior," *International Encyclopedia of Ergonomics and Human Factors*, 2nd ed., edited by W. Karwowski, Taylor and Francis, London, 2006, pp. 400–407.